Ore Geology Reviews 89 (2017) 876–886

Contents lists available at ScienceDirect

Ore Geology Reviews

journal homepage: www.elsevier.com/locate/oregeorev

The remaking of the Mengyejing potash deposit in Yunnan, China: Evidence from Rb-Sr isotopic systematics

Lijian Shen[a,b], Chenglin Liu[a,*], Jian-xin Zhao[b], Yuexing Feng[b], Licheng Wang[a], Jiaxi Zhou[b,c]

[a] MLR Key Laboratory of Metallogeny and Mineral Assessment, Institute of Mineral Resources, Chinese Academy of Geological Sciences, Beijing 100037, China
[b] Radiogenic Isotope Facility, School of Earth Sciences, The University of Queensland, Brisbane, QLD 4072, Australia
[c] State Key Laboratory of Ore Deposit Geochemistry, Institute of Geochemistry, Chinese Academy of Sciences, Guiyang 550002, China

ARTICLE INFO

Keywords:
Rb-Sr systematics
Potash deposit
Hydrothermal fluids
Multi-stage alteration

ABSTRACT

The Mengyejing potash deposit (MPD) is the first significant ancient potash deposit ever found in China, and it was considered to have formed during the middle to late Cretaceous. The $^{87}Sr/^{86}Sr$ ratios of potash bulk samples suggest that both bedded and veined potash orebodies of the MPD have been affected by igneous activity resulting from decompression melting of a metasomatically altered, depleted mantle from 16 Ma to present. The Rb-Sr isotopic systematics of the potash bulk samples define several apparent "isochrons" ranging from 0.609 ± 0.026 to 14.23 ± 0.63 Ma, with the maximum age being consistent with previous K-Ar ages of the K-bearing minerals from the MPD. Such isotopic signatures imply that the MPD may have been affected by multiple-stage fluid flow events since the mid-Miocene, consisting of hydrothermal fluids, continental fresh water, and/or hot spring water. It is very likely that the MPD is still affected by fluid flow-events in modern times. The mineral assemblage of halite + sylvite with minor amounts of carnallite was formed due to the recrystallization and diagenetic modification by hydrothermal fluids. Some characteristics of halite photomicrographs and inclusions and the lack of original halite chevron patterns are also supportive of the hypothesis that the deposit has undergone a diagenetic modification and dissolution–recrystallization processes.

1. Introduction

The MPD is located in the Simao basin in southwestern (SW) Yunnan, China, and only has a small proven reserve of 16.76 Mt (No. 16 Geological Brigade of Yunnan Province, 1980). Many key questions, such as the origin, the age of the formation and alterations after deposition, remain controversial. Ongoing studies of the MPD have led to the current opinion that the initial formation age is most likely middle-late Cretaceous (Yuan et al., 2013; Wang et al., 2015). Consensus has not been reached on the origin of the MPD, with several genetic models proposed (see Table 1). For instance, the MPD is interpreted as of marine origin based on evidence of Br geochemistry (Xu and Wu, 1983; Shuai, 1987; Gao et al., 2013), and a typical marine mineral: glauconite (No. 16 Geological Brigade of Yunnan Province, 1980). However, the MPD occurs in continental strata denoting that the potash itself has inevitably been provided by continental fresh water (Li et al., 2015). The studies of evaporite mineral trace elements by Xu and Wu (1983), and the characteristics and homogenization temperatures of halite fluid inclusions of the MPD (Yuan et al., 1991) indicate that the MPD has undergone late-stage dissolution and recrystallization after its formation.

The undeformed, bedded evaporites are thought to have the potential to preserve the original formation chemistry, both mineralogically and in fluid inclusions (Knauth and Beeunas, 1986; Das et al., 1990; Horita et al., 2002). In this case, evaporites commonly behave as closed systems until they are dissolved or rebuilt (Land et al., 1995). Ongoing studies of evaporite radiochemistry show that most evaporite minerals underwent continuing chemical reaction instead of remaining stable. Most data document a complex history of post-depositional modification, and only few data record the depositional age (Chaudhuri and Clauer, 1992). The evaporites, especially those subject to deep burial, may behave dynamically (Chipley and Kyser, 1989), and water-rock interactions during burial may control some aspects of the chemistry of saline formation water (Land et al., 1988; Land and Macpherson, 1992; Pauwels et al., 1993). Therefore, radiogenic isotopes can be used to constrain the metamorphic and hydrologic history of salt rocks rather than dating the initial sedimentation (Lippolt and Raczek, 1979). They can also be used to improve our understanding of both the depositional and the post-depositional history of the evaporites (Chaudhuri and Clauer, 1992).

* Corresponding author.
E-mail address: liuchengl@263.net (C. Liu).

http://dx.doi.org/10.1016/j.oregeorev.2017.07.025
Received 21 April 2017; Received in revised form 25 July 2017; Accepted 30 July 2017
Available online 31 July 2017
0169-1368/

Table 1
Different opinions on the genesis of the Mengyejing potash deposit.

	Viewpoints	Evidence
Salt sources	Major sources were seawater, with subordinate continental fresh water and minor amounts of deep hydrothermal fluids	Marine origin: Br geochemistry (Xu and Wu, 1983; Shuai, 1987; Gao et al., 2013), glauconite occurred in the potash deposit (No. 16 Geological Brigade of Yunnan Province, 1980) Continental fresh waters: the MPD occurred within continental strata; Deep hydrothermal fluids: hydrothermal-induced minerals (Gao et al., 2013), S isotopes and heavy metal elements of the MPD (Shuai, 1987), the MPD is located in a continental rift basin (Liu, 2013)
	Mixed sources with major continental fresh water, subordinate sea water and minor amounts of deep hydrothermal fluids	Mixed origin of continental fresh waters and seawater: The MPD occurred in continental strata, Br geochemistry, S, Sr and B isotopes of the MPD (Li et al., 2015); Deep hydrothermal fluids: The same as above
Origins and late alteration	The potash deposit has undergone late-stage dissolution and recrystallization after its formation during the process of brine evaporation	The characteristics and homogenization temperature of halite fluid inclusions of the MPD (Yuan et al., 1991), trace elements of evaporite minerals (Xu and Wu, 1983)

In this study, we focus primarily on potash ore bulk samples in an adit of the MPD and attempt to use the Rb-Sr isotopic systematics of chloride minerals (mostly halite and sylvite) to obtain a better understanding of post-depositional activity, such as the deformation and recrystallization caused by tectonic and igneous events.

2. Geologic background

The MPD is distributed over 3.5 km^2 within the Simao Basin (No. 16 Geological Brigade of Yunnan Province, 1980). The Simao basin is located in the southern part of the Lanping-Simao block (Fig. 1). The Lanping-Simao block is bordered to the west by the Jingdong and Nan suture zones and to the east and south by the Ailaoshan and Song Ma sutures, respectively (Wang et al., 2000; Metcalfe, 2006, 2009, 2011; Sone and Metcalfe, 2008). Rifting began on the eastern and western sides of the Simao Basin in the mid-Triassic, followed by a marine transgression. The study area was elevated and then denuded in the late Triassic (Chen et al., 2004). The Simao Basin became a Mesozoic-Cenozoic continental margin rift basin during the collision between the Eurasian and Indian plates (Liao and Chen, 2005). The entire Mesozoic-Cenozoic sedimentary fill consists of a thick sequence (~10,000 m) of red beds that evolved from marine and marine-continental sediments in the Triassic period to terrestrial sediments in the Jurassic-Cretaceous (Shuai, 2000). These red beds are unconformably overlain by the Late Cretaceous continental evaporites and clastic deposits of the Mengyejing Formation (Chen et al., 1995). The Mengyejing Formation consists of the following layers (Fig. 2), from bottom to top: (1) red muddy conglomerate, fine-grained sandstone and evaporites with

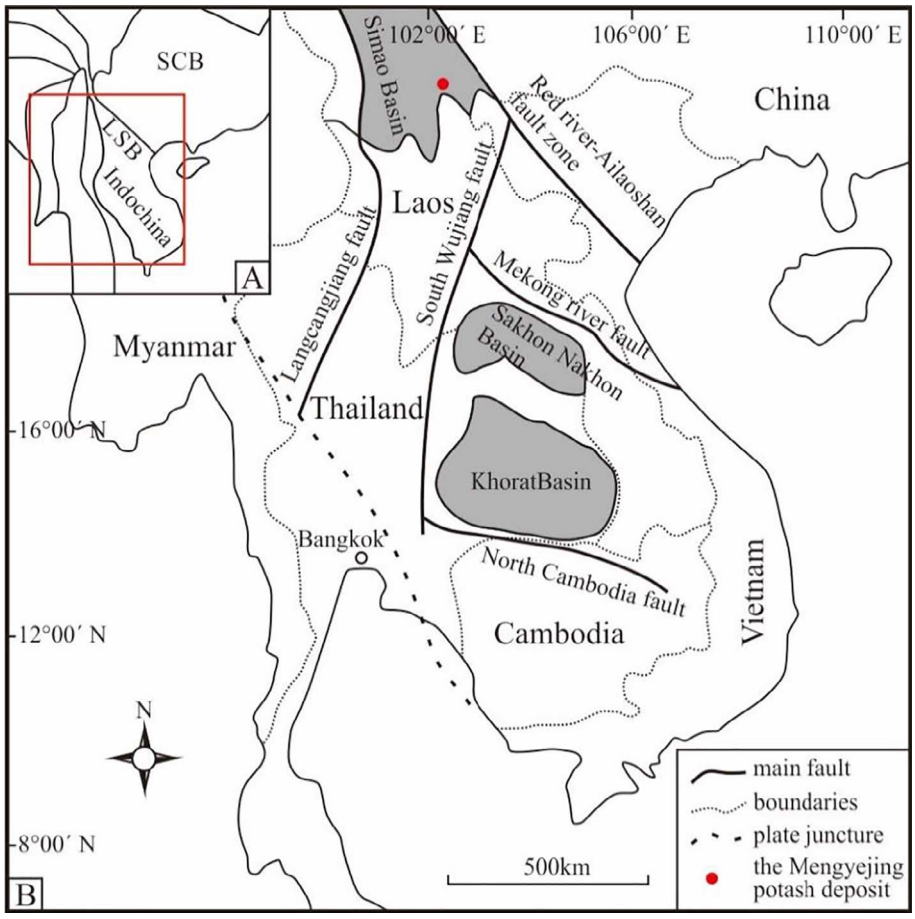

Fig. 1. A: Major tectonic units in the SE Tibetan Plateau (after Metcalfe, 2011) and B: regional geological setting of the study area (after El Tabakh et al., 1999). SCB: South China Block; LSB: Lanping-Simao Block.

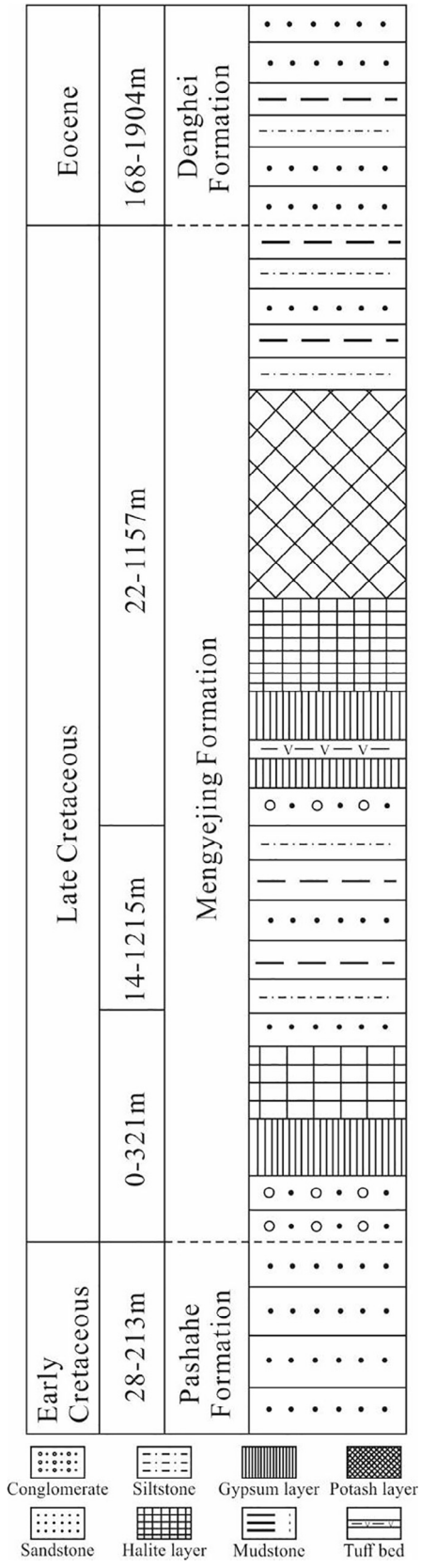

Fig. 2. Lithostratigraphic column of the Mengyejing Formation from which samples were collected (modified from Wang et al., 2015).

brown muddy fine-grained sandstone; (2) purplish fine-grained sandstone and mudstone; and (3) purplish conglomerate and medium- to fine-grained sandstone interlayered with evaporite sequences and tuff beds (Qu et al., 1998; Li et al., 2015).

3. Characteristics of the potash orebodies

The potash orebody of the MPD was highly deformed by tectonic movements (Fig. 3). Based on the stratigraphic, petrographic and geochemical evidence, potash ores (mainly chlorides) in the MPD can be divided into two major types:

(1) bedded potash ores with K contents of less than 10% (unpublished data) that contain a very small amount of clastics (Fig.4A);
(2) veined potash ores with K contents ranging from 0.72 to 27.59% (unpublished data) that contain a considerable amount of clastics (Fig. 4C)

3.1. Bedded potash orebodies

The bedded potash orebodies show banded light grey and white lithofacies with intense tectonic deformation where white layers of 1–10 cm in thickness alternate with light grey laminae, most of which are less than 1 cm in thickness (Fig. 4A). The banded potash orebodies consist mainly of chlorides, including halite and sylvite (Fig. 4B), and very small amounts of anhydrite and carnallite. The halite crystals are very clear, displaying atypical polygonal-mosaic texture, and lacking the typical primary depositional growth textures and fabric, i.e., chevron and cumulate crystals (Lowenstein and Spencer, 1990). Euhedral sylvite crystals act as cement filling voids within anhedral halite crystals (Fig. 4B). Halite is predominant within the bedded evaporites, followed by sylvite. Carnallite and anhydrite occur as minor minerals among or within the halite crystals. According to the petrographic studies, samples with K-bearing minerals (mainly sylvite) do not contain anhydrite, and samples with minor anhydrite do not contain any K-bearing minerals, either.

3.2. Veined potash orebodies

Veined potash orebodies are orange-red in color and coexist with many detrital components that generally consist of unconsolidated mudstones and siltstones. The interconnected veined potash orebodies penetrated the unconsolidated clastic components, forming a mesh-like structure (Fig.4C). The chloride minerals of the veined potash orebodies consist mostly of halite with a considerable amount of sylvite (Fig.4D) and a very small amount of carnallite. Those chloride minerals are very fine-grained and bondless. The sylvite crystals are usually smaller than halite crystals. The intergrowth of halite and sylvite with euhedral to sub-euhedral crystals encompasses the clastics (Fig.4D). Based on petrographic studies, the sylvite accounts for a higher proportion of the veined potash orebodies, in contrast to the bedded potash orebodies in which halite is greatly predominant.

4. Materials and methods

Samples for this study came from a horizontal section of an adit up to 500 m long within the MPD (Fig. 3). A total of 17 samples were collected, 14 of which are veined potash bulk samples, and 3 are from bedded potash layers. The veined potash bulk samples were handpicked under a binocular to obtain the chloride minerals halite and sylvite (the proportion of sylvite varies from less than 1% to ca. 20%). Bedded potash bulk samples were broken into small, millimetre-size fragments. Approximately 200 mg of each sample was digested with 0.1 N ammonium acetate (pH = 7–8) in a 5 ml Teflon beaker. Each solution was centrifuged and decanted after complete dissolution in order to eliminate the small amount of insoluble residue. All samples were split into aliquots by weight for analysis. One smaller aliquot was diluted and preserved for trace element analysis, and the other larger aliquot was acidified with 1 N HCl for column chemistry and strontium isotopic

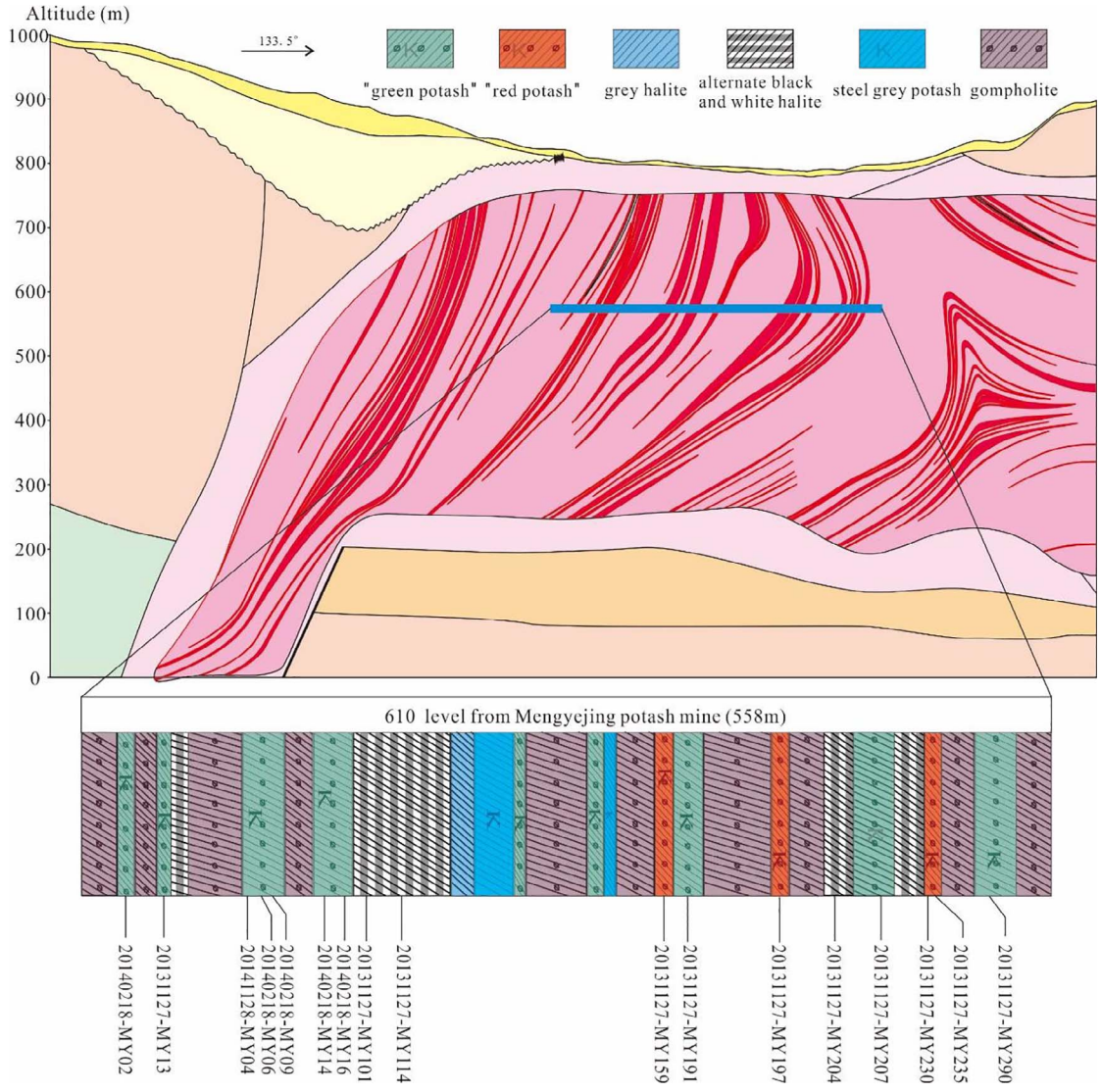

Fig. 3. The orebodies of the MPD and sampling section (modified from No. 16 Geological Brigade of Yunnan Province, 1980).

measurement. Strontium was separated and purified using a Sr-spec resin. The detailed information about Sr separation is given by Babechuk and Kamber (2011). The same procedure for was used REE collection. The Sr isotopic ratios were measured on a Nu Plasma multi-collector inductively coupled plasma mass spectrometer (MC-ICP-MS) in the RIF (Radiogenic Isotope Facility), The University of Queensland. Sr isotopic ratios were corrected for mass discrimination using $^{86}Sr/^{88}Sr = 0.1194$. Replicate analyses of separate loads of SRM987 yielded a mean $^{87}Sr/^{86}Sr = 0.710237 \pm 0.000027$ (2σ). Rb-Sr isotopic ratios were determined by a Thermo X-series II ICP-MS. The detailed procedure for ICP-MS trace element analysis is given in Niu and Batiza (1997). The two sigma errors for the $^{87}Rb/^{86}Sr$ ratio and $^{87}Sr/^{86}Sr$ ratio were estimated at ± 2.8% and ± 0.03%, respectively. Reference Rb-Sr isochron ages were calculated using the Isoplot/EX 3.75 software of Ludwig, 2012.

4.1. Rb and Sr chemistry

The analytical results of three bedded and fourteen veined potash bulk samples are summarized in Table 2. Rb concentrations in the bedded potash bulk samples range from 230 to 737 ppb, and Sr, from 17 to 44 ppb, respectively. Rb concentrations of the fourteen veined potash bulk samples have a wide variation, from 67 to 57,244 ppb, with 10,422 ppb on average. Similarly, their Sr concentrations vary widely from 13 to 5207 ppb, with 1575 ppb on average. Overall, most veined potash bulk samples are more enriched in Rb than bedded potash bulk samples, which is consistent with the fact that the veined potash bulk samples contain more K than bedded potash bulk samples.

4.2. Sr isotopic compositions

The $^{87}Sr/^{86}Sr$ ratios of the three bedded potash bulk samples are as follows: 0.706911 ± 0.000049 for sample 20131127-my101, 0.709474 ± 0.000046 for sample 20131127-my114, and 0.709665 ± 0.000016 for sample 20131127-my204. None of these is located in the range of the $^{87}Sr/^{86}Sr$ ratios of Cretaceous seawater (Hess et al., 1986; McArthur et al., 2001). The $^{87}Sr/^{86}Sr$ ratios of samples 20131127-my114 and 20131127-my204 are higher than those of Cretaceous seawater, and similar to those of adjoining continental waters of the MPD. For instance, the $^{87}Sr/^{86}Sr$ ratios of the Lancang river nearby the MPD range from 0.709736 to 0.713592 (Wu et al., 2009; Bo et al., 2015). The $^{87}Sr/^{86}Sr$ ratio of sample 20131127-my101 is lower than those of continental waters and Cretaceous seawater, denoting a deep origin.

The fourteen veined potash bulk samples have $^{87}Sr/^{86}Sr$ ratios ranging from 0.704976 to 0.710956, with an average of 0.7092121.

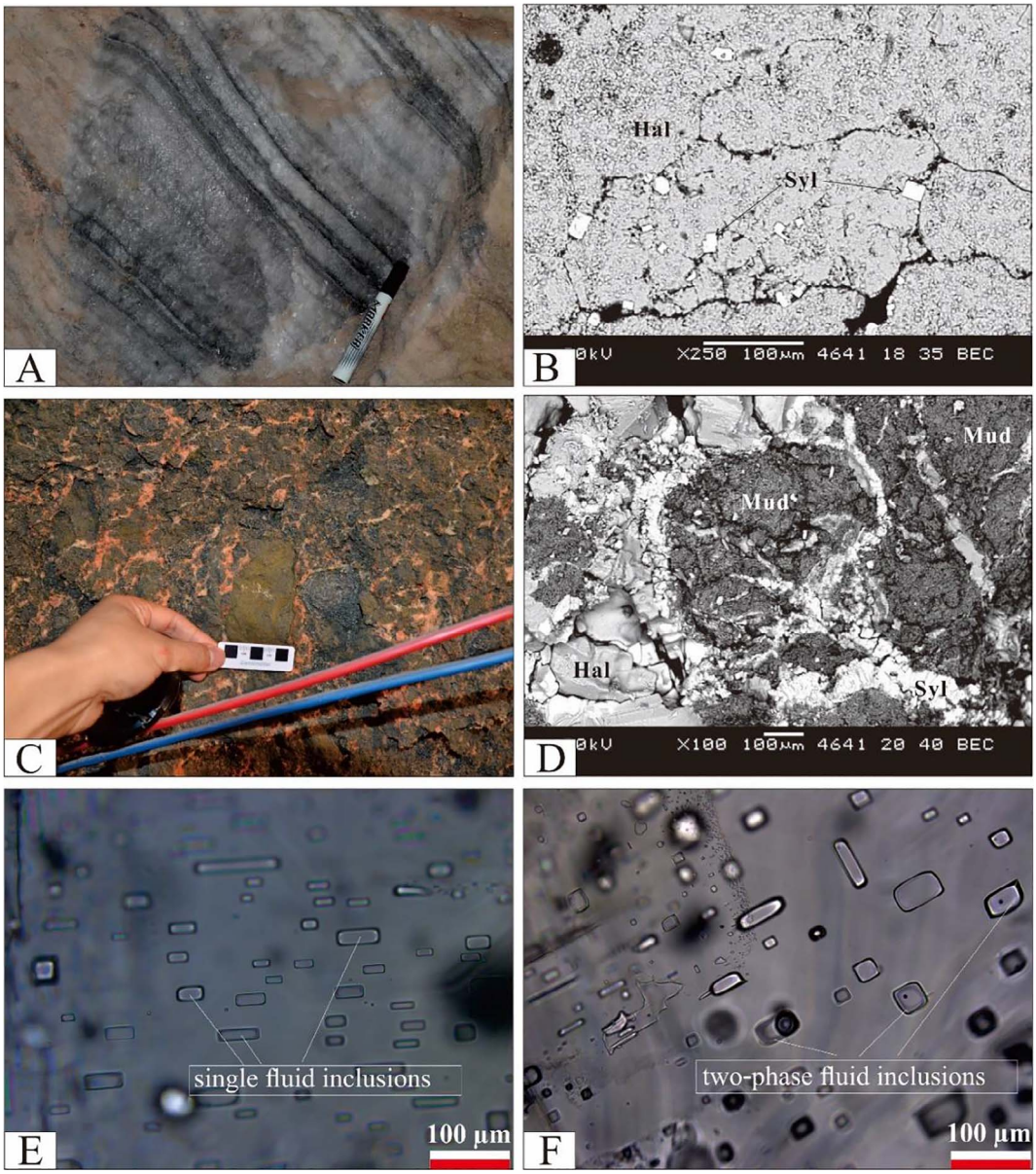

Fig. 4. Characteristics of potash ores and fluid inclusions in halite. A: alternate grey and white salt layers; B: backscattered electron image of bedded salt layers; C: coexisting vein-shaped potash and clastics; D: backscattered electron image of vein-shaped potash; E: characteristics of single fluid inclusions in halite; F: two-phase fluid inclusions in halite. Inclusion study from sample 20131127-MY101.

The $^{87}Sr/^{86}Sr$ ratios of most of them are higher than Cretaceous seawater, except for sample 20140218-my06 ($^{87}Sr/^{86}Sr$: 0.704976 ± 0.000016), which is extremely low compared to the rest of veined potash bulk samples and Cretaceous seawater, also denoting a deep origin. In addition to sample 20140218-my06, all the veined potash bulk samples have a narrow variation of $^{87}Sr/^{86}Sr$ ratios from 0.708697 to 0.710956, that is similar to or slightly lower than the adjoining continental fresh waters of the MPD.

5. Discussion

5.1. Constraints on the source of strontium

The MPD is constrained to have been deposited during Mid-Late Cretaceous time by U-Pb zircon ages of the tuff beds and sporopollenin from the Mengyejing formation containing the MPD (Wang et al., 2015; Yuan et al., 2013). The geochemistry of the bromide in chloride from the MPD has shown that the ore-forming brine is essentially derived from seawater (Gao et al., 2013). The compositions of the halite fluid inclusions from the MPD are Na-K-Ca-Mg-Cl type (Shen et al., 2017), which is consistent with brines from the evaporation of Cretaceous seawater.

Based on the study of McArthur et al. (2001), the $^{87}Sr/^{86}Sr$ ratios of seawater increased from 0.707437 to 0.707831 from the Middle to Late-Cretaceous (100.6 to 65.1 Ma BP), which is a relatively narrow range. Neither bedded nor veined potash bulk samples have $^{87}Sr/^{86}Sr$ ratios falling within this range.

It is shown from Table 2 that all samples contain a certain amount of rubidium, the ^{87}Rb to ^{87}Sr decay appears to increase $^{87}Sr/^{86}Sr$ ratios (Stein et al., 2000). If we assume that the potash orebodies have not been altered since their formation, the initial $^{87}Sr/^{86}Sr$ ratios of those potash bulk samples (including bedded and veined potash bulk samples) could be determined by using $^{87}Rb/^{86}Sr$ ratios, the present $^{87}Sr/^{86}Sr$ ratio of each sample, and the formation age. Based on the calculation with formation ages of 65.1 Ma and 100.6 Ma (Table 2), three samples with very low Rb concentrations and Rb/Sr ratios

Table 2
Rb and Sr contents and Sr isotope ratios of potash ore samples.

Type	Sample	Rb(ppb)	Sr(ppb)	$^{87}Rb/^{86}Sr$	$^{87}Sr/^{86}Sr$	"Initial" $^{87}Sr/^{86}Sr$ at	
						65.1 Ma	100.6 Ma
Bedded	20131127-my114	737	17	128.80	0.709474 ± 0.000046	0.590353	0.525349
	20131127-my101	230	44	15.31	0.706911 ± 0.000049	0.692751	0.685024
	20131127-my204	464	25	53.03	0.709665 ± 0.000016	0.660620	0.633856
Veined	20131127-my235	67	366	0.53	0.709174 ± 0.000011	0.708683	0.708416
	20131127-my13	568	13	125.09	0.709985 ± 0.000018	0.594295	0.531163
	20140218-my04	363	20	52.05	0.709366 ± 0.000020	0.661227	0.634958
	20131127-my191	99	265	1.09	0.708790 ± 0.000010	0.707781	0.707231
	20131127-my159	253	222	3.30	0.709021 ± 0.000010	0.705969	0.704303
	20140218-my02	178	35	14.72	0.708697 ± 0.000010	0.695083	0.687654
	20140218-my09	1962	175	32.43	0.709352 ± 0.000011	0.679359	0.662991
	20140218-my06	156	42	10.78	0.704976 ± 0.000016	0.695006	0.689565
	20131127-my197	312	3555	0.25	0.708821 ± 0.000018	0.708589	0.708463
	20131127-my207	36187	3725	28.10	0.710956 ± 0.000018	0.684967	0.670785
	20131127-my230	57244	3379	49.00	0.709681 ± 0.000025	0.664363	0.639633
	20131127-my290	17965	2119	24.52	0.710138 ± 0.000021	0.687460	0.675085
	20140218-my14	14711	5207	8.17	0.708975 ± 0.000025	0.701418	0.697295
	20140218-my16	15847	2929	15.65	0.709758 ± 0.000025	0.695284	0.687385

(including 20131127-my191, 20131127-my197 and 20131127-my235, see Table 2) have initial $^{87}Sr/^{86}Sr$ ratios ranging from 0.707781 to 0.708683 at 65.1 Ma, and 0.707231 to 708463 at 100.6 Ma. Although the "initial" $^{87}Sr/^{86}Sr$ ratios of these three samples are similar to Cretaceous seawater, they do not preclude post-depositional recrystallization. Thus, we cannot ascertain whether these three samples were originally derived from Cretaceous seawater. Based on the calculation, some other samples have "initial" $^{87}Sr/^{86}Sr$ ratios lower than 0.699 (Table 2), which is the initial value of a basaltic achondrite (Papanastassiou and Wasserburg, 1969). This calculation makes the hypothesis that the ore body of the MPD has not been altered since its formation unrealistic. Consequently, the orebodies must have been affected by late-stage activity.

Evaporite deposits are highly susceptible to post-depositional modification (Chaudhuri and Clauer, 1992). Apparently, the bedded and veined potash orebodies were both affected by hydrothermal fluids related to igneous activity with low $^{87}Sr/^{86}Sr$ ratios, because samples 20131127-my101 (bedded potash bulk sample) and 20140218-my06 (veined potash bulk sample) have $^{87}Sr/^{86}Sr$ ratios lower than those from Middle to Late Cretaceous seawater to the present (McArthur et al., 2001). Given that the decay of ^{87}Rb could accumulate radiogenic ^{87}Sr, the initial $^{87}Sr/^{86}Sr$ ratios should be even lower than the present values. Two episodes of igneous activity occurred during Cenozoic in the eastern Indo-Asian collision zone covering the MPD (Wang et al., 2001): (1) from 42 to 24 Ma (phase I in Fig. 5), with $^{87}Sr/^{86}Sr$ ranging from 0.705 to 0.710, (2) from 16 to 0 Ma (phase II in Fig. 5), with $^{87}Sr/^{86}Sr$ ranging from 0.703 to 0.705. If bedded potash orebodies were affected only by the early igneous activity with $^{87}Sr/^{86}Sr$ ratios ranging from 0.705 to 0.710 and no subsequent hydrothermal fluids affected the bedded potash orebodies, the "initial" $^{87}Sr/^{86}Sr$ ratios of some samples calculated based on phase I age range would be lower than a basaltic achondrite according the current $^{87}Rb/^{86}Sr$ and $^{87}Sr/^{86}Sr$ ratios of the bedded potash samples (Fig. 5), which is unrealistic. Thus, the only plausible explanation for such bedded potash Sr isotopic compositions for bulk samples is that their orebodies were affected by the younger igneous activity (phase II). However, it is not well known that if the bedded potash was affected thoroughly or partially, and whether the bedded potash was affected by previous fluid flow or not. Among the veined potash bulk samples, the $^{87}Sr/^{86}Sr$ ratio of sample 20140218-my06 (0.7049763) is lower than the early igneous activity (phase I) supporting the idea that veined potash orebodies were also affected by the younger igneous activity (phase II).

It is concluded that both bedded and veined potash orebodies have been altered by younger igneous activity (phase II) that was caused by the decompression melting of a metasomatically altered, depleted mantle (Wang et al., 2001). Except for samples 20131127-my101 and 20140218-my06, the rest have $^{87}Sr/^{86}Sr$ ratios ranging from 0.708697 to 0.710956 that are similar to or slightly lower than those of continental and hot spring waters nearby the MPD (Wu et al., 2009; Bo et al., 2015).

The orebodies of the MPD most likely originated from Cretaceous seawater (Gao et al., 2013; Shen et al., 2017). Thus, the potash orebodies inherited the Sr isotopic composition of Cretaceous seawater, and then they were altered by multi-stage fluid-flow events during post-depositional processes. The fluids might be of continental fresh water, hot spring water or/and hydrothermal fluids from deep crust or mantle. Consequently, the Sr isotopic mixing processes could have been caused by fluid events via a dissolution and recrystallization mechanism. The high contents of Rb in the potash layers would increase the amount of radiogenic ^{87}Sr, and then increase the $^{87}Sr/^{86}Sr$ ratios. The continental fresh water could also increase the $^{87}Sr/^{86}Sr$ ratios, as the $^{87}Sr/^{86}Sr$ ratios of continental fresh water are higher than those of seawater. The increased $^{87}Sr/^{86}Sr$ ratios were compensated for by the relatively low $^{87}Sr/^{86}Sr$ ratios of hydrothermal fluids, making the $^{87}Sr/^{86}Sr$ ratios of most samples not too high or too low (0.708687 to 0.710956). However, this cannot rule out the possibility that modern hot spring water and continental freshwater played a dominant role very recently other than hydrothermal fluids with low $^{87}Sr/^{86}Sr$ ratios. The Sr isotopic composition of active modern hot spring water and continental fresh water (the Lancang river) nearby the MPD ranges from 0.710673 to 0.713592 (Bo et al., 2015), and 0.709736 to 0.71020 (Wu et al., 2009), respectively. They are similar to those of most of the samples from the MPD.

5.2. Discussion on the Rb-Sr dating of the MPD

Three methods have been used to date evaporite minerals: K-Ar, K-Ca, and Rb-Sr dating (Geyh, 2012). Rb tends to be concentrated in K-rich minerals because Rb has chemical characteristics similar to K. Chlorides within the MPD contain potassium-bearing minerals (sylvite and carnallite) and thus have a potential for Rb-Sr dating.

Plotting the $^{87}Sr/^{86}Sr$ against the $^{87}Rb/^{86}Sr$ ratio for each sample shows that those points are quite scattered. Although this makes the precise interpretation of Rb-Sr isochron of those samples impossible, the data points show an overall increasing trend (Fig. 6). Several isochron ages have been determined subjectively based on the characteristics of the Rb-Sr isotopic systematics (Fig. 7): (1) isochron age of 4.29 ± 0.18 Ma, with an initial $^{87}Sr/^{86}Sr$ ratio of

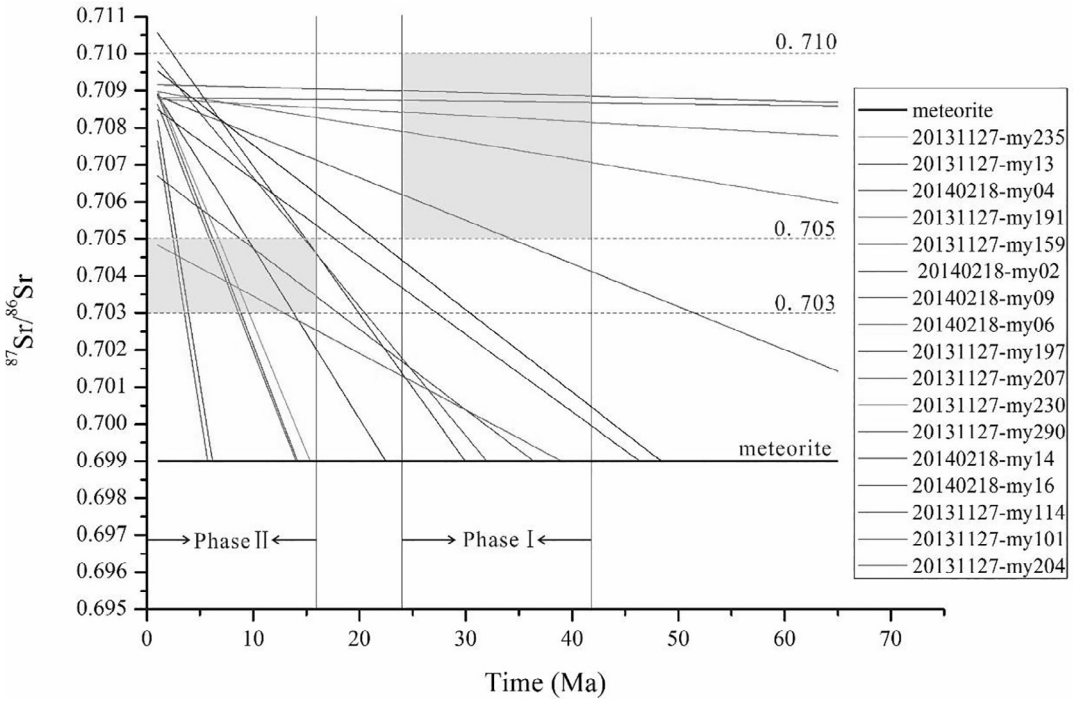

Fig. 5. Back-calculation of the initial $^{87}Sr/^{86}Sr$ ratios of potash salts from the MPD.

0.708816 ± 0.000012; (2) isochron age of 2.796 ± 0.089 Ma, with an initial $^{87}Sr/^{86}Sr$ ratio of 0.709152 ± 0.000011; (3) isochron age of 1.26 ± 0.28 Ma, with an initial $^{87}Sr/^{86}Sr$ ratio of 0.70879 ± 0.00011; (4) isochron age of 0.609 ± 0.026 Ma, with an initial $^{87}Sr/^{86}Sr$ ratio of 0.708909 ± 0.000024; and (5) isochron age of 24.6 ± 6.1 Ma, with an initial $^{87}Sr/^{86}Sr$ ratio of 0.7014 ± 0.0018. It seems that isochron (5) is less convincing because of its extremely low initial $^{87}Sr/^{86}Sr$ ratio (0.7014 ± 0.0018). It is even lower than that of the igneous activity of phase II, as mentioned earlier.

Except for two samples with relatively low $^{87}Sr/^{86}Sr$ ratios (sample 20131127-my101 and 20140218-my06), the rest of the 15 samples have a narrow range of $^{87}Sr/^{86}Sr$ ratios from 0.708697 ± 0.000010 to 0.710956 ± 0.000018, and the $^{87}Rb/^{86}Sr$ ratios of the 15 consistent samples (hereafter CS) range from 0.25 to 128.80. This dataset produced isochrons (1), (2), (3), and (4). These 4 isochron ages range from 0.609 ± 0.026 to 4.29 ± 0.18 Ma and are abnormally young compared with the formation age of the MPD.

Based on the Rb-Sr systematics of all samples, we can give limits to

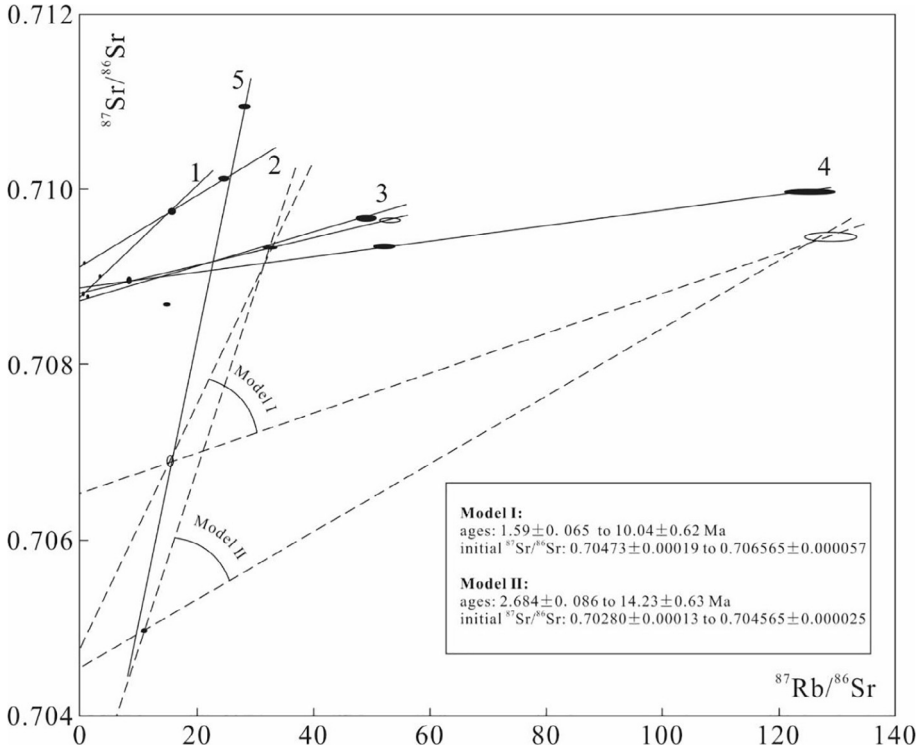

Fig. 6. Rb-Sr systematics of potash salts within the MPD.

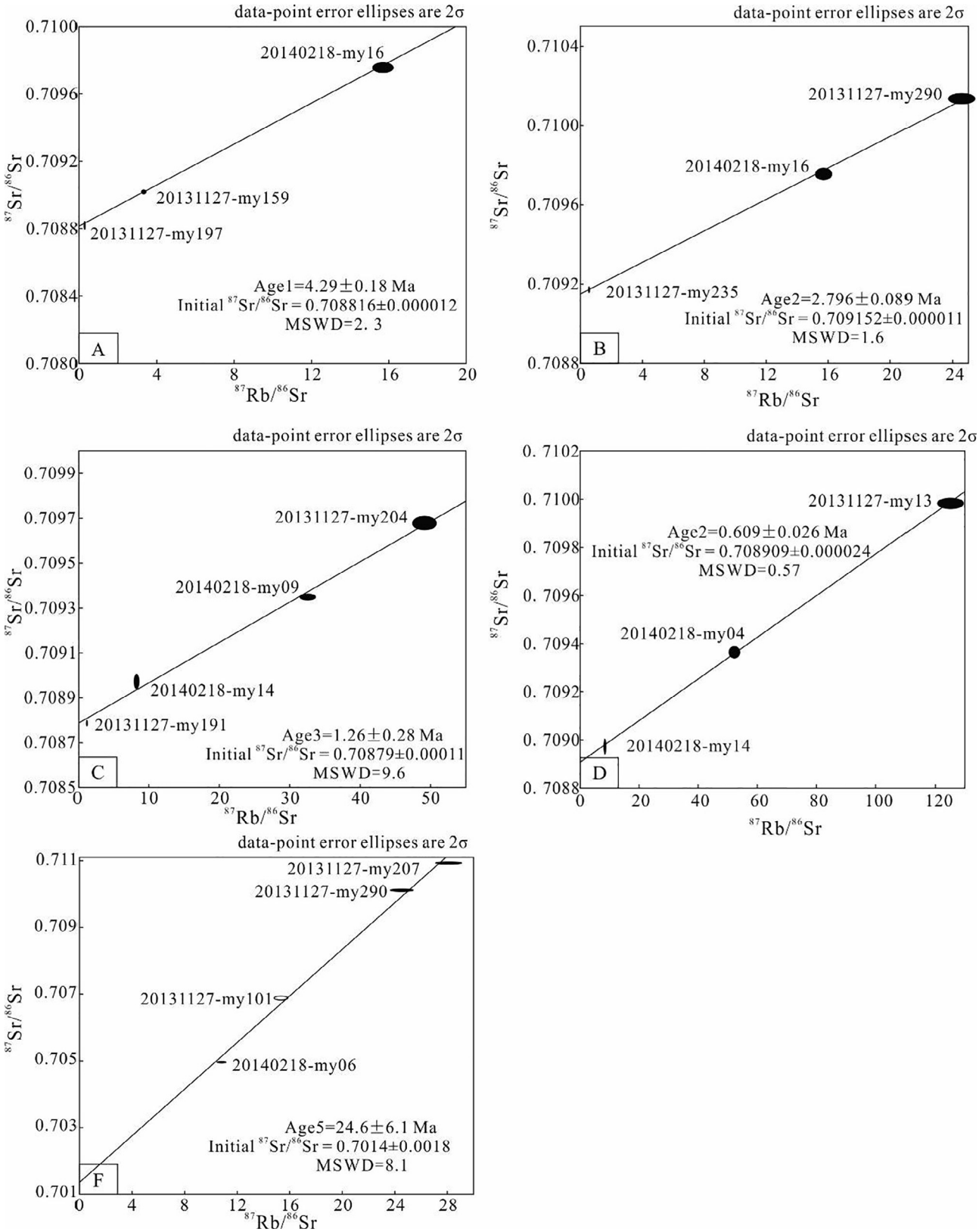

Fig. 7. Rb-Sr isochrones of different ages for all samples from the MPD. A: age 1 = 4.29 ± 0.18 Ma; B: age 2 = 2.796 ± 0.089 Ma; C: age 3 = 1.26 ± 0.28 Ma; D: age 4 = 0.609 ± 0.026 Ma; E: age 5 = 24.6 ± 6.1 Ma.

nominal Rb-Sr ages of the potash orebodies from the MPD, since the initial $^{87}Sr/^{86}Sr$ ratios should not be lower than 0.703, which is the minimum $^{87}Sr/^{86}Sr$ ratio of igneous activity phase II (Wang et al., 2001). This limiting parameter defined two ranges of ages (Fig. 6) based on sample 20131127-my101 (Model I) and sample 20140218-my06 (Model II). The isochron ages of Model I range from 1.59 ± 0.065 to 10.04 ± 0.62 Ma, with initial $^{87}Sr/^{86}Sr$ ratios ranging from 0.704730 to 0.706565. The isochron ages of Model II range from 2.684 ± 0.086

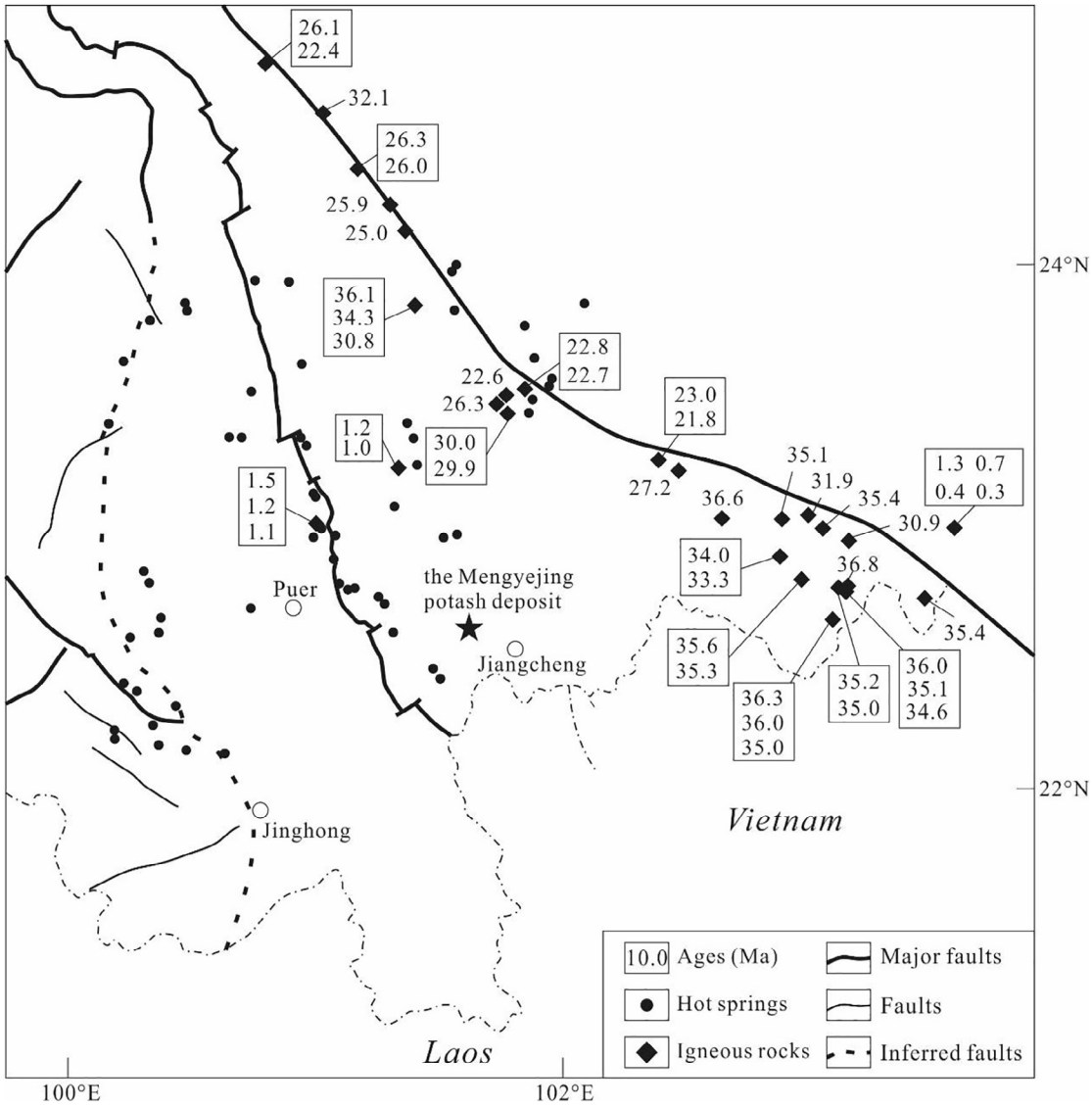

Fig. 8. Distribution of hot springs and magmatism in the vicinity of the MPD (modified from Wang et al., 2001; Zhao et al., 2014 and Deng et al., 2014).

to 14.23 ± 0.63 Ma, with initial $^{87}Sr/^{86}Sr$ ratios ranging from 0.702800 to 0.704565. The minimum ages of Models I and II are consistent with the isochron ages of the 15 CS (from 0.609 to 4.29 Ma). The maximum ages of Models I and II are somewhat similar to that of K-Ar ages of potash orebodies ranging from ca. 10.6 to 14.3 Ma (Shuai, 1987). The maximum isochron ages of the potash orebodies from the MPD fall in the Miocene, still much younger than the middle-late Cretaceous stratigraphic age.

5.3. The reactivity of the MPD

Many researchers found that Rb-Sr dates on sylvite, carnallite, and other K-bearing salt minerals are anomalously low compared to the stratigraphic ages (Lippolt and Raczek, 1979; Brookins et al., 1980; Register, 1979; Register and Brookins, 1980; Chaudhuri and Clauer, 1992). Because both Rb and Sr are relatively mobile elements, the isotopic system may readily be disturbed either by the influx of fluids or by a later thermal event. The Rb-Sr isochron ages of the MPD have an ambiguous meaning, suggesting that the salt minerals in the MPD have undergone very complex processes.

In contrast to the formation age of the MPD, this cluster of young Rb-Sr isochron ages is related to the complex diagenetic history of the evaporite minerals, which at least included dissolution and recrystallization of early-formed evaporite minerals and deformation of the salt layers. In addition, the original chevron patterns of halite crystals disappeared in the MPD, as evidenced by microphotographs (Fig.4E, F). The absence of the original halite crystal patterns may be due to recrystallization (Valyashko, 1956; Wardlaw and Schwerdtner, 1966).

As discussed above, the MPD should have been affected by the igneous activity of phase II with $^{87}Sr/^{86}Sr$ ratios ranging from 0.703 to 0.705 (Wang et al., 2001). Tectonic movements developed extensively after the formation of the MPD (No. 16 Geological Brigade of Yunnan Province, 1980) and created fractures through the evaporite sequence, allowing gas and brine to escape from their host formation below the evaporite sequences. When contacting the evaporite sequence, the brine dissolved the most soluble potash minerals and precipitated less soluble salts (Baar, 2013). On one hand, the high temperature hydrothermal fluids could dissolve more KCl than at lower temperatures. Thus, the brine would be K-enriched. On the other hand, the solubility of the KCl decreases sharply with decreasing temperature, and KCl is less soluble in halite-saturated brine than other potassium-magnesium minerals, such as carnallite (Land et al., 1995). Thus, KCl could easily precipitate from a halite-saturated brine during a cooling process compared with carnallite. The evaporite assemblage of halite + sylvite with minor amounts of carnallite in the MPD might be due to recrystallization and

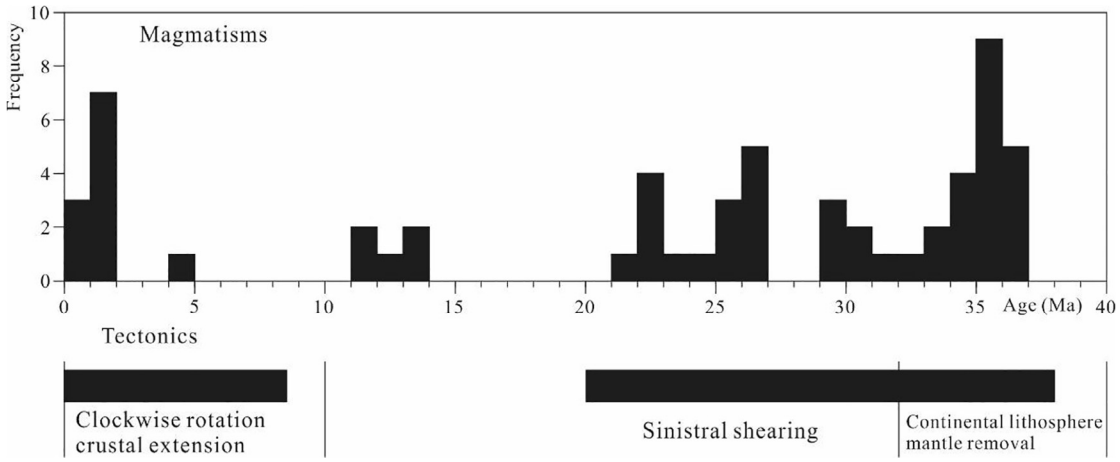

Fig. 9. Frequency of magmatism and tectonic events adjacent to the MPD during the Cenozoic (modified from Deng et al., 2014).

diagenetic modification by hydrothermal fluids.

Gas inclusions are widespread in halite (Fig. 4F). This could have been caused by the ascending brine that was accompanied by gas or/and the cooling of hydrothermal brine (Baar, 2013). The isochron ages suggest that the dissolution-recrystallization process appears to have begun by ca. 10–14 Ma ago. Subsequently, continental fresh water, spring water (Bo et al., 2015) and hydrothermal fluids have affected and altered the isotopic systems of the MPD continuously until the present. The hot springs are well-developed around the MPD at present (Zhao et al., 2014), and young igneous activity occurred approximately 1 ± 0.7 Ma based on Ar-Ar dating (Wang et al., 2001). It is very likely that the MPD has been affected by the igneous activity and hot springs adjacent to the MPD itself (Fig. 8). Furthermore, isochrons 3 and 4 are indicative of young igneous activity.

The scattered distribution of the data points referring to $^{87}Sr/^{86}Sr$ vs. $^{87}Rb/^{86}Sr$ also denotes that the MPD has been altered in-homogeneously by multiple fluid flow events that are caused by multi-stage magmatism and tectonic events (Fig. 9) in the adjacent Ailaoshan-Red river fault zone (Zhang et al., 2006; Deng et al., 2014) (Fig. 1). In general, it is practically impossible to know what the strontium would have evolved into and where it resided in each process. Thus, it is impossible to know whether the evaporites in the MPD have been affected by other events before the igneous activity of phase II, and how those fluid-flow events that specifically began at approximately 10–14 Ma ago may have affected the MPD.

6. Conclusions

(1) Both bedded and veined potash orebodies of the MPD have been affected by igneous activity caused by decompression-induced melting of a metasomatically altered, depleted mantle.
(2) The Rb-Sr systematics of the evaporites give several isochron ages ranging from 14.23 ± 0.63 to 0.609 ± 0.026 Ma, and the maximum isochron age is consistent with previous K-Ar ages of the evaporites in the MPD.
(3) The MPD has been affected inhomogeneously by multiple-stages of fluid flow events since the middle Miocene including hydrothermal fluids, continental fresh water, and hot spring water. Fluid flow events could have affected the MPD continuously to the present.

Acknowledgements

This work is supported by the National Key Project for Basic Research of China (No. 2011CB403007), and the National Natural Science Foundation of China (Nos. 41502080, 41572067). We would like to acknowledge Gong Daxing and Wang Di for their assistance in sampling.

References

Baar, C.A. (Ed.), 2013. Applied salt-rock mechanics 1: the in-situ behavior of salt rocks, vol. 16 Elsevier.
Babechuk, M.G., Kamber, B.S., 2011. An estimate of 1.9 Ga mantle depletion using the high-field-strength elements and Nd–Pb isotopes of ocean floor basalts, Flin Flon Belt, Canada. Precambr. Res. 189 (1), 114–139.
Bo, Y., Liu, C.L., Zhao, Y.J., Wang, L.C., 2015. Chemical and isotopic characteristics and origin of spring waters in the Lanping-Simao Basin, Yunnan, Southwestern China. Chemie der Erde-Geochemistry 75 (3), 287–300.
Brookins, D.G., Register, J.K., Register, M.E., Lambert, S.J., 1980. Long-term stability of evaporite minerals: geochronological evidence. In: Scientific Basis for Nuclear Waste Management. Springer, US, pp. 479–486.
Chaudhuri, S., Clauer, N., 1992. History of marine evaporites: constraints from radiogenic isotopes. In: Isotopic Signatures and Sedimentary Records. Springer, Berlin Heidelberg, pp. 177–198.
Chen, H.H., Dobson, J., Heller, F., Hao, J., 1995. Paleomagnetic evidence for clockwise rotation of the Simao region since the Cretaceous: a consequence of India-Asia collision. Earth Planet. Sci. Lett. 134 (1), 203–217.
Chen, Y.K., Liao, Z.T., Wei, Z.H., Li, M.H., 2004. Characteristics and tectonic evolution of the Lanping-Simao Mesozoic basin. Petrol. Geol. Exp. 26 (3), 219–222 (in Chinese with English abstract).
Chipley, D.B., Kyser, T.K., 1989. Fluid inclusion evidence for the deposition and diagenesis of the Patience Lake Member of the Devonian Prairie Evaporite Formation, Saskatchewan, Canada. Sediment. Geol. 64 (4), 287–295.
Das, N., Horita, J., Holland, H.D., 1990. Chemistry of fluid inclusions in halite from the Salina Group of the Michigan Basin: Implications for Late Silurian seawater and the origin of sedimentary brines. Geochim. Cosmochim. Acta 54 (2), 319–327.
Deng, J., Wang, Q.F., Li, J.G., Santosh, M., 2014. Cenozoic tectono-magmatic and metallogenic processes in the Sanjiang region, southwestern China. Earth Sci. Rev. 138, 268–299.
El Tabakh, M., Utha-Aroon, C., Schreiber, B.C., 1999. Sedimentology of the Cretaceous Maha Sarakham evaporites in the Khorat Plateau of northeastern Thailand. Sed. Geol. 123 (1), 31–62.
Gao, X., Fan, Q.F., Yao, W., Peng, Q., Dong, J., Qin, H., Di, Y.W., 2013. Genesis of the Mengyejing potash deposit in Lanping-Simao basin, Yunnan: Indication from the components of the deposit. Acta Geoscientica Sinica 34 (5), 529–536 (in Chinese with English abstract).
Geyh, M.A., Schleicher, H., 2012. Absolute age determination: physical and chemical dating methods and their application. Springer Science & Business Media.
Hess, J., Bender, M.L., Schilling, J.G., 1986. Evolution of the ratio of strontium-87 to strontium-86 in seawater from Cretaceous to present. Science 231 (4741), 979–984.
Horita, J., Zimmermann, H., Holland, H.D., 2002. Chemical evolution of seawater during the Phanerozoic: implications from the record of marine evaporites. Geochim. Cosmochim. Acta 66 (21), 3733–3756.
Knauth, L.P., Beeunas, M.A., 1986. Isotope geochemistry of fluid inclusions in Permian halite with implications for the isotopic history of ocean water and the origin of saline formation waters. Geochim. Cosmochim. Acta 50 (3), 419–433.
Land, L.S., Eustice, R.A., Mack, L.E., Horita, J., 1995. Reactivity of evaporites during burial: an example from the Jurassic of Alabama. Geochim. Cosmochim. Acta 59 (18), 3765–3778.
Land, L.S., Macpherson, G.L., 1992. Geothermometry from brine analyses: lessons from the Gulf Coast, USA. Appl. Geochem. 7 (4), 333–340.
Land, L.S., Macpherson, G.L., Mack, L.E., 1988. The geochemistry of saline formation waters, Miocene, offshore Louisiana. Gulf Coast Assoc. Geolog. Soc. Trans. 38, 503–511.
Li, M.H., Yan, M.D., Wang, Z.G., Liu, X.M., Fang, X.M., Li, J., 2015. The origins of the Mengye potash deposit in the Lanping-Simao Basin, Yunnan Province, Western China. Ore Geol. Rev. 69, 174–186.
Liao, Z.T., Chen, Y.K., 2005. Nature and evolution of Lanping-Simao basin prototype. J.

Tongji Univ. (Nat. Sci.) 33 (11), 1527–1531 (in Chinese with English abstract).
Lippolt, H.J., Raczek, I., 1979. Cretaceous Rb-Sr total rock ages of Permian salt rocks. Naturwissenschaften 66 (8), 422–423.
Liu, C.L., 2013. Characteristics and formation of potash deposits in continental rift basins: a review. Acta Geoscientica Sinica 34 (5), 515–527 (in Chinese with English abstract).
Lowenstein, T.K., Spencer, R.J., 1990. Syndepositional origin of potash evaporites; petrographic and fluid inclusion evidence. Am. J. Sci. 290 (1), 1–42.
Ludwig, K.R. 2012. User's Manual for Isoplot 3.75: a Geochronological Toolkit for Microsoft Excel. Berkeley Geochronology Centre, Berkeley. Special Publication No. 5.
McArthur, J.M., Howarth, R.J., Bailey, T.R., 2001. Strontium isotope stratigraphy: LOWESS version 3: best fit to the marine Sr-isotope curve for 0–509 Ma and accompanying look-up table for deriving numerical age. J. Geol. 109 (2), 155–170.
Metcalfe, I., 2006. Palaeozoic and Mesozoic tectonic evolution and palaeogeography of East Asian crustal fragments: the Korean Peninsula in context. Gondwana Res. 9 (1–2), 24–46.
Metcalfe, I., 2009. Late Paleozoic and Mesozoic tectonic and palaeogeographical evolution of SE Asia. Geolog. Soc., London, Special Publ. 315 (1), 7–23.
Metcalfe, I., 2011. Palaeozoic-Mesozoic history of SE Asia. Geol. Soc., London, Special Publ. 355 (1), 7–35.
Niu, Y., Batiza, R., 1997. Trace element evidence from seamounts for recycled oceanic crust in the Eastern Pacific mantle. Earth Planet. Sci. Lett. 148 (3), 471–483.
No. 16 Geological Brigade of Yunnan Province, 1980. Detailed Exploration Geological Reports of Mengyejing Potash Deposit of Jiangcheng County, Yunnan Province. Kunming: No. 16 Geological Brigade of Yunnan Province (in Chinese).
Papanastassiou, D.A., Wasserburg, G.J., 1969. Initial strontium isotopic abundances and the resolution of small time differences in the formation of planetary objects. Earth Planet. Sci. Lett. 5, 361–376.
Pauwels, H., Fouillac, C., Fouillac, A.M., 1993. Chemistry and isotopes of deep geothermal saline fluids in the Upper Rhine Graben: Origin of compounds and water-rock interactions. Geochim. Cosmochim. Acta 57 (12), 2737–2749.
Qu, Y.H., Yuan, P.Q., Shuai, K.Y., Zhang, Y., Cai, K.Q., Jia, S.Y., Chen, C.D., 1998. Potash-Forming Rules and Prospects of Lower Tertiary in Lanping-Simao Basin, Yunnan. Geological Press, Beijing pp. 1–120 (In Chinese with English abstract).
Register, J.K., 1979. Rubidium-Strontium and Related Studies of the Salado Formation, Southeastern New Mexico. University of New Mexico (Master's thesis).
Register, J.K., Brookins, D.G., 1980. Rb-Sr isochron age of evaporite minerals from the Salado formation (Late Permian), southeastern New Mexico. Isochron. Isochron West 29, 39–42.
Shen, L.J., Liu, C.L., Wang, L.C., Hu, Y.F., Hu, M.Y., Feng, Y.X., 2017. Degree of brine evaporation and origin of the Mengyejing potash deposit: evidence from fluid inclusions in halite. Acta Geologica Sinica (English Edition) 91 (1), 175–185.
Shuai, K.Y., 1987. Geologic-tectonic evolution and evaporite formation of Mesozoic-Cenozoic era in Yunnan. Geoscience 1 (2), 207–229 (in Chinese with English abstract).
Shuai, K.Y., 2000. New explanation of genesis of the Meso-Cenozoic Lanping-Simao Basin. Earth Sci. Front. 7 (4), 380 (in Chinese).
Sone, M., Metcalfe, I., 2008. Parallel Tethyan sutures in mainland Southeast Asia: new insights for Palaeo-Tethys closure and implications for the Indosinian orogeny. Compte Rendus Geosci. 340 (2), 166–179.
Stein, M., Starinsky, A., Agnon, A., Katz, A., Raab, M., Spiro, B., Zak, I., 2000. The impact of brine-rock interaction during marine evaporite formation on the isotopic Sr record in the oceans: evidence from Mt. Sedom, Israel. Geochim. Cosmochim. Acta 64 (12), 2039–2053.
Valyashko, M.G., 1956. Geochemistry of bromine in the processes of salt deposition and the use of the bromine content as a genetic and prospecting criterion. Geochemistry 6, 570–589.
Wang, J.H., Yin, A., Harrison, T.M., Grove, M., Zhang, Y.Q., Xie, G.H., 2001. A tectonic model for Cenozoic igneous activities in the eastern Indo-Asian collision zone. Earth Planet. Sci. Lett. 188 (1), 123–133.
Wang, L.C., Liu, C.L., Fei, M.M., Shen, L.J., Zhang, H., Zhao, Y.J., 2015. First SHRIMP U-Pb zircon ages of the potash-bearing Mengyejing Formation, Simao Basin, Southwestern Yunnan, China. Cretac. Res. 52, 238–250.
Wang, X.F., Metcalfe, I., Jian, P., He, L.Q., Wang, C.S., 2000. The Jinshajiang-Ailaoshan suture zone, China: tectonostratigraphy, age and evolution. J. Asian Earth Sci. 18 (6), 675–690.
Wardlaw, N.C., Schwerdtner, W.M., 1966. Halite-anhydrite seasonal layers in the middle Devonian Prairie evaporite formation, Saskatchewan, Canada. Geolog. Soc. Am. Bull. 77 (4), 331–342.
Wu, W.H., Yang, J.D., Xu, S.J., Li, G.J., Yin, H.G., Tao, X.C., 2009. Sr fluxes and isotopic compositions of the eleven rivers originating from the Qinghai-Tibet Platea and their contributions to $^{87}Sr/^{86}Sr$ evolution of seawater. Sci. China, Ser. D Earth Sci. 52 (8), 1059–1067.
Xu, X.S., Wu, J.L., 1983. Potash deposits in Mengyejing, Yunnan—A study of certain characteristics, geochemistry of trace elements and genesis of the deposits. Bull. Chinese Acad. Geolog. Sci. 5, 17–36 (in Chinese with English abstract).
Yuan, J.Q., Cai, K.Q., Xiao, R.G., Chen, H.Q., 1991. The characteristics and genesis of inclusions in salt from Mengyejing potash deposit in Yunnan province. Earth Sci.—J. China Univ. Geosci. 16 (2), 137–143 (in Chinese with English abstract).
Yuan, Q., Qin, Z.J., Wei, H.C., Sheng, S.R., Shan, F.S., 2013. The ore-forming age and palaeoenvironment of the Mengyejing formation in Jiangcheng, Yunnan Province. Acta Geoscientica Sinica 34 (5), 631–637 (in Chinese with English abstract).
Zhang, J.J., Zhong, D.L., Sang, H.Q., Zhou, Y., 2006. Structural and geochronological evidence for multiple episodes of deformation since Paleocene along the Ailaoshan-Red river shear zone, Southeastern Asia. Chinese J. Geol. 41 (2), 291–310 (in Chinese with English abstract).
Zhao, C.P., Chen, Y.L., Wang, Y., Zhou, Z., 2014. Geothermal field in the uppermost crust in the Ning'er-Tongguan volcanic zone, Southwest China: Implications for tectonics and magmatism. Acta Petrologica Sinica 30 (12), 3645–3656 (in Chinese with English abstract).